

HIGH-CYCLE FATIGUE IN MICRON-SCALE STRUCTURAL FILMS OF POLYCRYSTALLINE SILICON: A REACTION-LAYER FAILURE MECHANISM

C. L. Muhlstein^{1*}, E. A. Stach², and R. O. Ritchie^{1*}

¹Materials Sciences Division, Lawrence Berkeley National Laboratory, and Department of Materials Science and Engineering, University of California, Berkeley, CA 94720

²National Center for Electron Microscopy, Lawrence Berkeley National Laboratory, Berkeley, CA 94720

Abstract—A study has been made of high-cycle fatigue in 2- μm thick structural films of n^+ -type, polycrystalline silicon for MEMS applications. Using an “on-chip” test structure resonating at ~ 40 kHz, such thin-film polysilicon is shown to display “metal-like” stress-life fatigue behavior in room air environments, with failures occurring after lives in excess of 10^{11} cycles at stresses as low as half the fracture strength. Through *in-situ* monitoring of the natural frequency to evaluate the damage evolution by notch-root oxidation and cracking, and using transmission electron microscopy to image such damage, it is concluded that the mechanism of thin-film silicon fatigue involves sequential oxidation and environmentally-assisted cracking in the native SiO_2 layer. This moisture-induced “reaction-layer fatigue” mechanism can also occur in bulk silicon but it is only significant in thin films where the critical crack size for catastrophic failure can be reached by a crack growing within the oxide layer. The susceptibility of thin-film silicon to fatigue failure is shown to be suppressed by the use of alkene-based self-assembled monolayer coatings that prevent the formation of the native oxide.

Keywords: Silicon; Fatigue; Thin films, MEMS; Self-assembled monolayer coatings

1. Introduction

The promise of revolutionary commercial products at nano-scale dimensions has fueled the rapid development of microelectromechanical systems (MEMS) and the enabling technologies of surface micromachining. Silicon-based structural films have emerged as the dominant material system for MEMS because the micromachining technologies for silicon are readily adapted from the microelectronics industry and are compatible with fabrication

* To whom correspondence should be addressed: Tel.: 001 510 486-4584, 5798; fax: 001 510 486-4995.

E-mail addresses: cmuhlstn@uclink4.berkeley.edu (C.L. Muhlstein); roritchie@lbl.gov (R.O. Ritchie)

strategies for integrated circuits necessary for actuation and control. However, the long-term durability of these microsystems may be compromised by susceptibility of thin-film silicon to premature failure by fatigue at ambient temperatures [1-9].

Cyclic fatigue is the most commonly encountered mode of failure in structural materials, occurring in both ductile (metallic) and brittle (ceramic) solids (although the mechanisms are quite different) [10]. The mechanistic understanding of fatigue together with the use of damage/fracture mechanics to describe its effect at continuum dimensions has allowed for the reliable design and operation of innumerable macro-scale structures, such as aircraft airframes and engines. At the micro-scale, the fatigue of ductile materials is attributed to cyclic plasticity involving dislocation motion that causes alternating blunting and resharpening of a pre-existing crack tip as it advances [11]. In contrast, brittle materials invariably lack dislocation mobility at ambient temperatures, such that fatigue occurs by cycle-dependent degradation of the (extrinsic) toughness of the material in the wake of the crack tip [12]. However, the relevance of these fatigue mechanisms to silicon films has yet to be established.

Silicon is generally regarded as a prototypical brittle material; dislocation activity is generally not observed at low homologous temperatures (below $\sim 500^\circ\text{C}$) and there is little evidence of extrinsic toughening, such as by grain bridging or microcracking [13]. Moreover, silicon is not susceptible to environmentally-induced cracking (stress-corrosion cracking) in moist air or water [14-16] at growth rates measurable in bulk specimens. *These observations strongly suggest that silicon should not fatigue at room temperature.* Indeed, there has been no evidence to date that bulk silicon is susceptible to fatigue failure. However, there is substantial evidence that cyclically-stressed micron-scale films of silicon can fail at stresses well below the (single-cycle) fracture strength [1-9, 17].

Connally and Brown first reported the fact that fatigue cracks can initiate and grow in silicon thin films in room temperature air a decade ago [1]. Since then, the present authors and others [2-8] have confirmed that 2 to 20 μm thick single crystal and polycrystalline silicon films can prematurely fail in fatigue, at stresses as low as half their (single-cycle) fracture strength (after fatigue lives in excess of $\sim 10^{11}$ cycles). Despite such results, the mechanistic origins of the fatigue of thin-film silicon have remained elusive. Early studies highlighted the importance of water vapor and speculated that the mechanism may be associated with static fatigue of the native silica layer [1, 8]. Other explanations have

involved dislocation activity in thin films (e.g. [18]), stress-induced phase transformations [5], and impurity effects [5], although in no instances has conclusive experimental evidence been presented to support any of these mechanisms. Moreover, there has never been any direct observation of fatigue damage in micron-scale silicon, nor indications on how it accumulates.

A recent study by the authors [19], however, provided the initial experimental evidence that the crack initiation and growth processes involved in the fatigue of silicon are confined to the amorphous SiO_2 reaction layer that forms upon exposure to air. In the current work, we present a mechanism for this behavior, termed reaction-layer fatigue, on the basis of stress-life fatigue data, numerical models of the damage accumulation, and microstructural analysis using high-voltage transmission electron microscopy. Additionally, we present a method for suppressing the cyclic fatigue of silicon through the use of alkene-based, self-assembled monolayer coatings.

2. EXPERIMENTAL PROCEDURES

The thin-film silicon was fabricated as 2- μm thick films from the first structural polysilicon layer on run 18 of the MCNC/Cronos MUMPs™ process. This standard micromachining process for this foundry is based on the low-pressure chemical vapor deposition (LPCVD) of n^+ -type (resistivity, $\rho = 1.9 \times 10^{-3} \Omega \cdot \text{cm}$) polycrystalline silicon [20]. Wafer curvature measurements showed the film to have a compressive residual stress of about 9 MPa [20]; out-of-plane deformation due to a through-thickness residual stress gradient could not be detected using white-light interferometry. Secondary ion mass spectroscopy (SIMS), referenced to known standards, was used to quantify the concentration of hydrogen, carbon, oxygen, and phosphorous present. The films were found to be representative of materials used throughout micromachining and MEMS research and production.

The elastic properties of polysilicon thin films approach the average behavior of idealized polycrystalline materials. An average of the Voigt and Reuss bounds for a random, polycrystalline aggregate (Young's modulus, $E = 163 \text{ GPa}$, Poisson's ratio, $\nu = 0.23$ [21]) can be considered as a useful estimate of the elastic behavior of the system. The fracture strength typically ranges from 3 to 5 GPa depending on loading condition, specimen size, and test technique. The fracture toughness, K_{IC} , is $\sim 1 \text{ MPa}\sqrt{\text{m}}$ [13, 22].

The microstructure of the films was characterized using transmission electron microscopy (TEM). Cross-sectional TEM specimens were prepared from the patterned films using standard laboratory practices [23]. Pairs of patterned chips containing the surface micromachined structures were glued together face-to-face, mechanically thinned, dimpled, and ion milled to the desired electron transparency. Diffraction contrast and high-resolution microscopy of these specimens was performed using the Berkeley JEOL Atomic Resolution Microscope (ARM) at an operating voltage of 800 kV and a JEOL 3010 TEM operating at 300 kV. Analytical characterization was accomplished using a Philips CM200 Field Emission microscope equipped with a Link Energy Dispersive Spectrometer (EDS) and a Gatan Image Filter for electron energy loss spectroscopy (EELS) and energy filtered imaging (EFTEM). Plan view observations of the grain morphology and oxide structure were accomplished using both the ARM and the Kratos High Voltage Electron Microscope (HVTEM) operating at 0.8-1.0 MeV. Plan view samples were prepared by simply lifting the surface micromachines off of the substrate using a tungsten probe tip and placing them onto 100 mesh clam shell grids. For HVTEM studies, no additional thinning was necessary to image through the entire 2 μm thick samples.

To determine the fatigue life as a function of applied stress, a notched cantilever beam specimen was used (Fig. 1). Specimens were ~ 40 μm long, 19.5 μm wide, and 2 μm thick, with a 13 μm deep notch (~ 1 μm root radius) located 9.8 μm from the base. Two groups of samples were prepared by first removing the sacrificial oxide layer in 49% hydrofluoric acid (HF) for 2½ and 3 min, respectively [6]. After drying at 110°C in air, the samples were mounted in ceramic electronic packages and ultrasonically wire bonded for testing. Prior to cycling, each test structure was run for over 10^7 cycles at ~ 450 MPa to verify system performance and to screen for abnormalities from fabrication, packaging or handling.

In an attempt to suppress formation of the native oxide and access of moisture to the silicon surface, specific specimens were coated with self-assembled monolayers (SAMs) after release in hydrofluoric acid. Surfaces were coated with an alkene-based monolayer of 1-octadecene, $\text{C}_{16}\text{H}_{33}\text{CH}=\text{CH}_2$. This was achieved by creating a hydrogen-terminated surface using aqueous HF during a 3 min sacrificial oxide removal and applying the SAM in a reactor containing a solution of one part 1-octadecene in nine parts hexadecane [24]. This

hydrophobic SAM bonds directly to the hydrogen-terminated surface atoms of the silicon film such that no oxide can form; it acts as an effective barrier to both oxygen and water [24].

The stress-life (S/N) fatigue behavior of the polysilicon films was investigated using a micron-scale “on-chip” fatigue characterization structure, which is $\sim 300\ \mu\text{m}$ square and $2\ \mu\text{m}$ thick (Fig. 1a). The notched cantilever beam specimen is attached to a large, perforated plate that serves as a resonant mass. The mass and beam are electrostatically forced to resonate and the resulting motion is measured capacitively. On opposite sides of the resonant mass are interdigitated “fingers” (“comb drives”); one side is for electrostatic actuation, the other provides capacitive sensing of motion. The specimen is attached to an electrical ground, and a sinusoidal voltage (with no direct-current (DC) offset) at the appropriate frequency is applied to one comb drive, thereby inducing a resonant response in the plane of the figure. These conditions generate fully reversed, constant amplitude, sinusoidal stresses at the notch, i.e., a load ratio (ratio of minimum to maximum load) of $R = -1$, that are controlled to better than 1% precision. The opposing comb drive is attached to a constant potential difference, and the relative motion of the grounded and biased fingers induces a current proportional to the calibrated amplitude of motion [6]. The small, induced current is converted to a DC voltage using an analog circuit, the output of which is proportional to the stress amplitude, $\sigma_a = \frac{1}{2}(\sigma_{\max} - \sigma_{\min})$, where σ_{\max} and σ_{\min} are, respectively, the maximum and minimum stresses.

Specimens were cycled to failure at resonance with a frequency of $\sim 40\ \text{kHz}$ in ambient air ($\sim 25^\circ\text{C}$, 30-50% relative humidity) at stress amplitudes ranging from 2 to 4 GPa using the control scheme described in refs. [5, 6]. The specimen compliance, computed from change in the natural frequency of the system [6], was monitored *in situ* to evaluate the evolution of damage in the sample from cracking and oxide formation. Experiments using an unnotched specimen have been used to demonstrate that such changes in resonant frequency are a result of such damage and are not due to changes in temperature, relative humidity or accumulation of debris [8, 25]. Throughout the test, the response of the system was found to remain linear, i.e., the opening and closing stiffnesses were essentially identical. This implies the absence of any significant fatigue crack closure during crack growth, contrary to early studies [8, 25] on the fatigue of silicon films where closure had been postulated.

The relationship between stresses in the vicinity of the notch and its dynamic response was determined numerically. Measured displacements and finite element modeling were used

to calculate the maximum principal stress amplitude at the notch. Additionally, finite element methods were used to evaluate the natural frequency, compliance, and stress-intensity factor, K , for structures containing cracks. The numerical models were constructed using a commercial software package (ANSYS v 5.7); full details are reported in ref. [26].

S/N fatigue data were analyzed by applying the finite element models to experimentally measured displacement (stress) amplitudes. The time to failure was determined by a loss of resonance of the structure and the elapsed cycles to failure determined from the average natural frequency in a given time window. The crack length at a given point in time was determined from the change in natural frequency again using the finite element models [26]. Crack-growth rates were determined using a modified secant method applied over ranges of crack extension of 2 nm with 50% overlap of the previous calculation window; the average crack-growth rate was calculated based on a linear fit of the experimental data. The maximum stress intensity immediately prior to failure was taken as an estimate of the fracture toughness of the material.

After testing, the crack path and fracture surfaces of the specimens were characterized using scanning electron microscopy (SEM) and HVTEM. To avoid corrupting any microstructural or fractographic features, neither SEM conductive coatings nor TEM thinning processes were used.

To evaluate the possibility of specimen heating with the kHz fatigue testing, high-resolution infrared (IR) imaging of the fatigue characterization structure was performed *in situ* in order to map temperature changes during testing. Thermal images were generated by plotting the difference between IR images (12-bit resolution) collected while the structure was resonated at the indicated stress amplitude, and at rest. Individual IR images were collected by averaging over 2 sec at an acquisition rate of 50 Hz. Temperature changes as small as 20 mK could be detected with a spatial resolution of better than 8 μm .

3. RESULTS

3.1. Microstructural analysis

The microstructure of the 2- μm thick polycrystalline silicon film, shown in plan and cross sectional TEM images in Fig. 2, revealed an equiaxed grain morphology (grain size of ~ 100 nm), with no evidence of strong texture (from corresponding selected-area diffraction). No

variations in microstructure were apparent near features such as the root of the notch. The lack of a textured columnar structure, which is routinely observed in thin-film silicon [27], may be a result of the 900°C annealing used to dope the silicon with phosphorous which allows the residual stresses associated with growth of the film to relax.

SIMS analysis of the contaminants present revealed the interior of the film to contain $\sim 2 \times 10^{18}$ atoms/cm³ hydrogen, 1×10^{18} atoms/cm³ oxygen, and 6×10^{17} atoms/cm³ carbon [6], levels which are consistent with the processing history of the film. In addition, 1×10^{19} atoms/cm³ of phosphorous were detected, from the phosphosilicate glass used to dope the film. Oxygen concentrations in excess of $\sim 10^{18}$ atoms/cm³ at room temperature can be associated with precipitation of amorphous and crystalline Si-O phases [28], although EELS of the interior of the grains revealed no segregation of oxygen or carbon in the film. Similarly, EFTEM imaging revealed no segregation of oxygen, carbon, phosphorous or nitrogen within the detectability limits of the technique. We conclude that that no precipitation of secondary species exists in the films.

Diffraction contrast imaging was used to characterize the defect structure of the film. A relatively high magnification weak-beam dark field image of one representative grain is presented as Fig. 3a. This image was taken by tilting the sample to a strong 220 diffraction condition near a $\langle 110 \rangle$ zone axis in the film and imaging with the weakly diffracting $\bar{2}20$ beam. This particular imaging condition is particularly sensitive to strain in the lattice, with the bright areas in this image indicating regions that are highly strained [29]. In Fig. 3b, a higher magnification 220 bright field image of the interior of this grain shows several different types of lattice defects, including microtwins, stacking faults and Lomer-Cottrell dislocation locks (Figs. 3c,d). In each instance, the bright areas of contrast in Fig. 3a corresponded to one of these types of lattice defects, and not to the presence of precipitates.

3.2. Stress-life fatigue behavior

Stress-life (S/N) data for these polysilicon films is shown in Fig. 4, based on a total of 28 fatigue specimens tested in room air; lives, N_f , varied from ~ 10 sec to 34 days (3×10^5 to 1.2×10^{11} cycles) for stress amplitudes ranging from ~ 2 to 4 GPa at $R = -1$ [6]. Fifteen of the samples were exposed to HF for 2½ min during the release procedure and the remaining thirteen samples for 3 min; no significant difference in behavior was observed. The silicon films can be seen to display “metal-like” S/N behavior, with an endurance strength at 10^9 -

10^{10} cycles of roughly half the (single-cycle) fracture strength. Similar behavior has been seen in 20- μm thick films of single-crystal silicon cycled under identical conditions [5].

3.3. *Monitoring of damage*

The change in resonant frequency of the cantilever beam was monitored during each test to provide a continuous measure of the specimen compliance. This frequency decreased monotonically (by as much as 50 Hz in the long-life tests) before eventual specimen failure at the notch (Fig. 5), behavior that suggests that the failure of the film occurs after progressive accumulation of damage, e.g., by the stable propagation of a crack. Indeed, the longer the life of the specimen, the larger the decrease in beam stiffness. The link between changes in resonant frequency and damage processes is examined in ref. [6] and is summarized below.

Based on experimental observations, the frequency change was reasoned to be due to localized oxidation and cracking at the notch root and was analyzed using plane-stress finite element modal analyses with ANSYS [6]. The model suggested that for ~ 1 nm of crack extension, a 1 Hz change in natural frequency should be observed. The corresponding model for local notch root oxidation predicted an initial decrease in frequency with increasing oxide layer thickness (at a rate very similar to that induced by cracking) due to the relatively low elastic modulus of the SiO_2 ; specifically, a 1 nm increase in oxide thickness resulted in a ~ 0.5 Hz decrease in resonant frequency. The numerical models imply that the measured changes in resonant frequency are consistent with processes occurring on length scales commensurate with the native oxide thickness; indeed, estimates of the crack length are also plotted in Fig. 5 and reveal crack sizes less than 50 nm throughout the entire fatigue test. These analyses provide support to the notion that damage is accumulated during the fatigue test from notch root oxidation and cracking. As described below, HVTEM studies in the present work provide direct confirmation of this hypothesis.

3.4. *Fractography and crack-path analysis*

SEM and TEM of both failed specimens and specimens interrupted during testing were used to evaluate such damage, including the nature of the crack trajectory and the fracture surface morphology. Previous work [6] established that crack paths in polycrystalline silicon films during fatigue and subsequent overload failure are transgranular. Scanning electron

microscopy at magnifications as high as 80,000X revealed a cleavage fracture mode with few distinctions in fracture surface morphology in the (presumed) fatigue and overload regimes.

Overload fractures: Overload fracture surfaces were (unambiguously) created by manually loading the fatigue test structure with a fixed (non-cyclic) displacement under an optical microscope; these conditions generate cracks that arrest due to the decreasing stress gradient associated with displacement-control in this geometry. Cracking in the silicon was confirmed to be transgranular cleavage (Fig. 6), with evidence of secondary cracking and microcracking consistent with the “slivers” which appear on fracture surfaces (Fig. 6b).

Fatigue fractures: Although SEM studies were inconclusive in discerning any differences in the fatigue and overload fractures, the distinct nature of these two processes was clearly evident in the HVTEM. Examination of failed fatigue specimens and untested control samples revealed a stark difference in the native oxide found at the notch root. In the control samples, a native oxide of ~30 nm in thickness was uniformly distributed over the surfaces of the sample, including the notch. While thick compared to the native oxide that will typically develop on single crystal silicon at room temperature [30-33], the presence of heavy phosphorous doping and elevated temperature exposure during drying of the film created a significantly thicker reaction layer. 30-nm thick native oxide layers were also present on the tested fatigue sample, except in the vicinity of the notch where the oxide layer was significantly thicker. Specifically, up to a three-fold increase in oxide thickness at the root of the notch was observed on samples that had been exposed to cyclic stresses (Fig. 7), a result confirmed on three different fatigued samples. Such enhanced notch-root oxidation was not observed on non-cyclically loaded samples. As it is conceivable that the high loading frequency and induced currents may induce heating in the notch region, the role of thermal effects in the oxidation process was experimentally evaluated.

High-resolution (20 mK) infrared images were taken of the test structure during cyclic loading; results at rest and at increasing stress amplitude are shown in Fig. 8. Each image was created by plotting the difference between the IR image at rest and resonating at load; the vertical scale represents temperature changes less than 1 K [19]. The slight warming of the mass originates from friction of the silicon with air as the structure resonates at ~40 kHz. However, the temperature of the structure does not rise significantly (<1K) above ambient, and there is no measurable change in temperature of the notched region. The absence of

heating in the cantilever beam section clearly indicates that the enhanced notch-root oxidation is not thermally induced. Conversely, as the notch root is (initially) the most highly stressed region of the structure, the process appears to be mechanical in origin and, since it is not observed under quasi-static loading, associated with the cyclic loading.

The precise nature of this mechanically-enhanced oxidation is at present unclear. The notion of a mechanical driving force for oxidation is already a central feature of models for the oxidation of silicon [34-39]. The presence of a compressive stress in the oxide primarily due lattice and thermal mismatch is thought to be responsible for the details of shape effects in oxidation as well as the initially high oxidation rates observed during the early stages of oxide growth [34-39]. However, as most studies have been performed at high temperature, the role of stress in room temperature oxidation and the importance of cyclic loading are far less clear. Studies on the effect of geometry on oxidation would suggest that the oxide at the notch root should be *thinner* than that found on flat surfaces[38, 39]; this further implies the critical role of stress. Furthermore, it is generally accepted that stress can modify the diffusivity of a species in a given material [40]; indeed, high-temperature oxidation studies in silicon suggest contributions on the order of 5 to 10% of the stress-free activation energy for thermally grown oxides [34-37]. At room temperature, these changes in activation energy would lead to a change in oxidation rate of more than 40 times. As the residual stress distribution in the oxide is dependent on the growth conditions, including the applied stress, it is conceivable that the time-varying stresses encountered during fatigue loading play a role in the oxide thickening. Additionally, the presence of the stress induces cracks within the oxide layer at the notch root, which permits the further ingress of moisture and continued oxidation in this region.

Despite the uncertainty in the origin of the thickened notch-root oxide layer, its role in the fatigue of thin film silicon is far clearer. By interrupting fatigue specimens prior to failure after testing at various stress amplitudes and examining them with HVTEM, several small cracks (on the order of tens of nanometers in length) were observed within the native oxide at the notch root (Fig. 9). The fact that these cracks were partially through the oxide layer indicates that they are stable cracks; indeed, this is the first evidence of stable fatigue cracking in silicon. Moreover, the size of the cracks was consistent with the compliance change of the sample predicted from the finite element modeling.

It is reasoned that the cause of the cracking in the oxide layer is stress-corrosion cracking due to the moist air environment. Since the toughness of the SiO_2 oxide ($K_c \sim 0.8 \text{ MPa}\sqrt{\text{m}}$) is comparable to that of the silicon ($K_c \sim 1 \text{ MPa}\sqrt{\text{m}}$), it is unlikely that the oxide would crack prematurely and certainly not in the stable manner shown in Fig. 9. However, unlike silicon, amorphous SiO_2 is susceptible to environmentally-assisted cracking in moist environments; indeed, the threshold stress intensity, K_{sc} , for such cracking is much less than K_c , i.e., typically $K_{\text{sc}} \sim 0.25 \text{ MPa}\sqrt{\text{m}}$, in contrast to silicon where $K_{\text{sc}} \approx K_c$ [14-16]. Indeed, such effects have recently been suggested for subcritical crack growth in borosilicate glass [41]. Since no evidence of dislocation activity near the crack surface nor phase transformations in the vicinity of the notch root was detected, the fatigue of structural silicon films in ambient air is deemed to be associated with stress-corrosion cracking in the native oxide layer that has been thickened under cyclic loading (reaction-layer fatigue).

3.5. Fracture mechanics analysis

Crack-growth rates: As noted above, *in situ* measurements of the change in natural frequency during the fatigue test were used to determine the crack length, a , as a function of time or cycles [26]. From such data, crack-growth rates, da/dN , were calculated over increments of 2 nm in crack extension; results in the form of da/dN as a function of a are shown in Fig. 10. Crack lengths during the fatigue process can be seen to remain under ~ 50 nm, consistent with the fatigue process occurring in the oxide layer. Growth rates are vanishingly small* and progressively decrease with increasing crack length during the test, akin to behavior observed for microstructurally-small cracks, cracks growing under displacement control, cracks growing into residual stress fields, and cracks approaching interfaces. In the present case, the effect is likely related to several of these factors acting *in concert*, as the cracks are certainly small in size, conditions do pertain to displacement control, some degree of residual compression will exist in the SiO_2 layer, and the crack advancing in the oxide is approaching the SiO_2/Si interface where the elastic mismatch between the relatively compliance oxide and the three-fold stiffer silicon substrate will cause the crack to decelerate [43].

* The absolute values of these crack-growth rates are clearly physically unrealistic. However, the growth rates reported are average values associated with the number of cycles at 40 kHz for the crack to grow over 2 nm increments, assuming that the crack is growing continuously. Although this is the standard way of computing fatigue-crack growth rates [42], in reality the crack is either not propagating every cycle or the crack front is not advancing uniformly.

This behavior provides insight into the observed S/N behavior of thin-film silicon. In metals, the gradual increase in life with decreasing stress amplitude is a direct consequence of the relatively wide range of stable crack growth, characterized by a low crack-growth rate exponent of $m \approx 3-5$ in the Paris law, $da/dN = \Delta K^m$ (where ΔK is the stress-intensity range). The appearance of a wide range of lives for brittle materials tested at the same stress amplitude (e.g. [44]) is a natural result of the size distribution of flaws and the limited range for stable fatigue-crack growth in the material, i.e., a large crack-growth rate exponent, $m > 10$ [10]. It is believed that the metal-like S/N behavior of silicon is a direct consequence of the decreasing crack-growth rates observed as the crack extends in the oxide layer. Because of the range of stable crack growth, the decreasing the driving force results in a failure in a measurable timeframe. Although arising from different mechanisms, the correlation between stress amplitude and fatigue life in metals and silicon films is ultimately due to the range of stable crack growth within the timeframe of the tests.

Fracture toughness and critical crack size: If the crack-driving force at failure is taken as an estimate of the fracture toughness, the toughness of the material can be determined. The crack length estimates at failure were used with plane-strain models of the stress intensity for the notched cantilever beam structure; the relationship between crack length, applied forces, and the stress intensity are detailed in [26]. Results from the polysilicon fatigue tests (Fig. 11) give an average fracture toughness of $\sim 0.85 \text{ MPa}\sqrt{\text{m}}$, consistent with that of the native oxide [45]. However, it is important to note the relationship between the critical crack size at final failure, a_c , where $K = K_c$, and the thickness, h_o , of the SiO_2 reaction layer. Such critical crack sizes are estimated in Fig. 12 for the range of maximum principal stresses used in this investigation. It is apparent that for applied stresses of 2 to 4 GPa, which caused failure in the present films after 10^5 to 10^{11} cycles, the critical crack sizes are less than 50 nm, i.e., comparable, or less than, the observed oxide layer thicknesses (i.e., $a_c \leq h_o$). *This indicates that the entire fatigue-crack initiation and propagation process and the onset of catastrophic (overload) failure all occur within the oxide layer.*

4. DISCUSSION

4.1. Reaction-layer fatigue

The cyclic fatigue of brittle materials is usually associated with the degradation of (extrinsic) toughening mechanisms in the crack wake [10]. Such toughening arises from crack-tip shielding, which in brittle (non-transforming) ceramic materials generally results from mechanisms such as grain bridging. Under cyclic loading, frictional wear in the sliding grain boundaries can lead to a progressive decay in the bridging stresses (e.g., refs. [10, 46, 47]). The fatigue of brittle materials is therefore invariably associated with intergranular failure. When such materials fail transgranularly, e.g., as in commercial SiC and sapphire [48, 49], there is generally little or no susceptibility to fatigue failure. Since polycrystalline silicon always fails transgranularly [6, 22, 50], and there has been no reported evidence of extrinsic toughening mechanisms, the material would not be expected to be prone to cyclic fatigue. Similarly, below $\sim 500^\circ\text{C}$, there is no evidence of mobile dislocation activity [51, 52], which could cause fatigue failure as in a ductile material.

In the present work, we have demonstrated that the fatigue susceptibility of thin-film silicon is associated with a conceptually different mechanism, that of sequential mechanically-induced oxidation and environmentally-assisted cracking of the surface layer of native oxide that forms upon reaction with the atmosphere, a mechanism that we term *reaction-layer fatigue*. This mechanism of fatigue damage, shown schematically in Fig. 13, was observed experimentally as a continuous decrease in the stiffness of the specimen during fatigue loading [6] and was visualized directly using HVTEM. The native oxide, which initially forms on the exposed silicon surface with a thickness and composition dictated by the environment and processing history and then thickens in high stress regions during subsequent fatigue loading, becomes the site for stress-corrosion cracks which grow stably through the oxide layer. The process then repeats itself until a critical crack size is reached, whereupon the silicon itself fractures catastrophically by transgranular cleavage. The rate-dependence of thin-film silicon fatigue failures is thus dictated by the cycle-dependent oxide thickening process and the time-dependent environmentally-assisted subcritical crack growth in this oxide layer.

The reaction-layer mechanism applies equally to bulk as well as thin-film silicon, even though bulk silicon is generally not considered to be susceptible to either stress-corrosion

cracking or fatigue. This is because cracking in the nano-scale native oxide film would have a negligible effect on a macroscopic sample of silicon under load, since crack sizes in the oxide could never reach the critical size, i.e., $a_c \gg h_o$, where h_o is the native oxide thickness. In contrast, with micro- and nano-scale samples where the surface-to-volume ratio is far larger such that the oxide layer represents a large proportion of the sample, cracks within the oxide film are readily able to exceed the critical crack size, i.e., $a_c \leq h_o$. Consequently, cracking in the oxide layer can lead to failure of the entire silicon component.

4.2. Suppression of reaction-layer fatigue

The central treatise of this paper is that the fatigue of thin-film silicon is environmentally induced. Thus, the obvious test of this mechanism is to test in an environment where the native oxide cannot form. This poses certain difficulties with the present system as the removal of the atmosphere affects the damping of the system, causing a mechanical as well as an environmental effect on cracking behavior [26]. An alternative strategy is to use self-assembled monolayer (SAM) coatings to suppress the formation of the native oxide with the expectation that such samples would not be susceptible to fatigue in air.

Such coatings have been developed by Maboudian *et al.* [24, 53] to reduce the friction coefficient between contacting silicon surfaces. In the present work, an alkene-based SAM coating of 1-octadecene was used; the 3 nm thick monolayer on the polysilicon at the root of the notch is shown in Fig. 14. These coatings are applied directly after the silicon is removed from the HF, and bond directly with the hydrogen-terminated silicon surface; accordingly, they suppress the formation of the native oxide (Fig. 14). Moreover, they are hydrophobic, stable up to 400°C, and provide an effective surface barrier to both moisture and oxygen.

The fatigue behavior of thin films of silicon coated with this and other SAM coatings is currently under study. However, initial results on the alkene-based SAM-coated films do show fatigue lifetimes that are not affected by cyclic stresses (Fig. 15a). Indeed, comparisons of coated and uncoated samples indicate that damage accumulation is dramatically altered and fatigue lives are significantly extended in the coated samples (Fig. 15b). This result clearly provides strong support for the proposed mechanism of silicon fatigue.

5. CONCLUSIONS

Based on a study of the high-cycle fatigue of 2- μm thick structural films of LPCVD n^+ -type polycrystalline silicon for MEMS applications, the following conclusions can be made:

1. Micron-thick thin films of polysilicon silicon can degrade and prematurely fail by high-cycle fatigue in room air environments. Measured stress/life behavior at 40 kHz was seen to be “metal-like”, with failures occurring at stresses as low as half the (single-cycle) fracture strength for lives in excess of 10^9 cycles. This presents a significant limitation for the long-term stability and durability of silicon-based MEMS devices.
2. High-voltage transmission electron microscopy (HVTEM) of the polysilicon thin-film samples revealed a native SiO_2 oxide layer some 30 nm thick. However, during fatigue cycling, this layer was thickened by a factor of roughly three in the immediate vicinity of the notch root. As high-resolution IR measurements revealed that the temperature of the notch did not exceed 1 K above ambient, such enhanced notch-root oxidation was considered to be primarily mechanically-induced.
3. By periodically stopping fatigue tests for microscopic examination, HVTEM also revealed the presence of stable cracks, tens of nanometers in length, within the enhanced oxide layer. Such subcritical crack growth was reasoned to occur by moisture-induced stress-corrosion cracking in the amorphous SiO_2 .
4. *In situ* monitoring of the change in natural frequency of the test structure during fatigue testing was found to be consistent with such progressive evolution of damage in the form of oxide formation and subcritical cracking. Fracture mechanics based calibrations using finite element methods revealed cracks sizes not exceeding 50 nm, comparable with those imaged directly with HVTEM. This implies that the entire fatigue phenomenon, involving fatigue crack initiation, subcritical cracking, and the onset of catastrophic failure, occurs wholly within the native oxide layer.
5. Accordingly, the fatigue of thin-film polysilicon is ascribed to a “surface reaction-layer” mechanism, specifically involving mechanically-induced oxide thickening and stress-corrosion cracking of the resulting oxide film.
6. Such reaction-layer fatigue is also applicable to bulk silicon although in comparison to thin-film silicon, its effect will be negligible. This is because the high surface-to-volume ratio of the micron-scale thin films means that the critical crack size for the onset of

catastrophic fracture (when $K = K_c$) will occur for cracks within the oxide film. In contrast, the corresponding critical crack size for bulk silicon will be much larger than the native oxide thickness.

7. The susceptibility of thin-film polysilicon to premature failure by high-cycle fatigue can be suppressed through the use of alkene-based self-assembled monolayer coatings. Such hydrophobic coatings, which bond directly to the hydrogen-terminated silicon surface (directly following HF etching), completely inhibit the formation of the oxide layer and further act to prevent the ingress of both moisture and oxygen.

Acknowledgements-This work was funded by the Director, Office of Science, Office of Basic Energy Research, Materials Sciences Division of the U.S. Department of Energy under Contract No. DE-AC03-76SF00098 (for E.A.S. and R.O.R.), and by Exponent, Inc., Natick, MA (for C.L.M.). The authors wish to thank Dr. S.B. Brown for his support, Dr. W. Van Arsdell for the original specimen design, Prof. R. Maboudian and W.R. Ashurst for assistance with the self-assembled monolayer technologies, Drs. M. Enachescu and S. Belikov for help with the IR imaging, and Prof. R.T. Howe and Dr. J.M. McNaney for helpful discussions.

REFERENCES

1. Connally, J.A. and Brown, S.B., *Science*, 1992, **256**, 1537-39.
2. Brown, S.B., Van Arsdell, W. and Muhlstein, C.L., in *Proceedings of International Solid State Sensors and Actuators Conference (Transducers '97)*, ed. S. Senturia, IEEE, 1997, pp. 591-93.
3. Muhlstein, C. and Brown, S., in *Proceedings of the NSF/AFOSR/ASME Workshop on Tribology Issues and Opportunities in MEMS*, ed. B. Bhushan, Kluwer Academic, Dordrecht, The Netherlands, 1997, pp. 80.
4. Muhlstein, C.L., Brown, S.B. and Ritchie, R.O., in *Materials Science of Microelectromechanical System (MEMS) Devices III*, eds. H. Kahn, M. de Boer, M. Judy, and S.M. Spearing, MRS, Pittsburgh, PA, 2000, pp. EE5.8.1-EE5.8.6.
5. Muhlstein, C.L., Brown, S.B. and Ritchie, R.O., *JMEMS*, 2001, in press.
6. Muhlstein, C.L., Brown, S.B. and Ritchie, R.O., *Sensors and Actuators A*, 2001, in press.

7. Kahn, H., Ballarini, R., Mullen, R.L. and Heuer, A.H., *Proc. Roy. Soc. A*, 1999, **455**, 3807-23.
8. Van Arsdell, W.W. and Brown, S.B., *JMEMS*, 1999, **8**, 319-27.
9. Komai, K., Minoshima, K. and Inoue, S., *Micros. Tech.*, 1998, **5**, 30-37.
10. Ritchie, R.O., *Int. J. Fract.*, 1999, **100**, 55-83.
11. Suresh, S., *Fatigue of Materials*, 2nd ed., Cambridge University Press, Cambridge, England, 1998.
12. Ritchie, R.O. and Dauskardt, R.H., *J. Ceram. Soc. Jap.*, 1991, **99**, 1047-62.
13. Kahn, H., Tayebi, N., Ballarini, R., Mullen, R.L. and Heuer, A.H., in *Transducers '99: 10th International Conference on Solid State Sensors and Actuators*, Elsevier, Oxford, UK, 1999, pp. 274-80.
14. Chen, T.J. and Knapp, W.J., *J. Am. Ceram. Soc.*, 1980, **63**, 225-26.
15. Lawn, B.R., Marshall, D.B. and Chantikul, P., *J. Mater. Sci.*, 1981, **16**, 1769-75.
16. Wong, B. and Holbrook, R.J., *J. Electrochem. Soc.*, 1987, **134**, 2254-56.
17. Allameh, S.M., Gally, B., Brown, S. and Soboyejo, W.O., in *Materials Science of Microelectromechanical System (MEMS) Devices III*, eds. H. Kahn, M. de Boer, M. Judy, and S.M. Spearing, MRS, Pittsburgh, PA, 2000, pp. EE2.3.1-EE2.3.6.
18. Kato, N.I., Nishikawa, A. and Saka, H., in *Advanced Characterisation of Semiconductor Materials*, Elsevier, Oxford, UK, 2000, pp. 113-15.
19. Muhlstein, C.L., Stach, E.A. and Ritchie, R.O., *Appl. Phys. Let.*, 2001, in review.
20. MCNC/Cronos, www.memsrus.com, 2000.
21. Simmons, G. and Wang, H., *Single Crystal Elastic Constants and Calculated Aggregate Properties: a Handbook*, 2nd ed., M.I.T. Press, Cambridge, MA, 1971.
22. Ballarini, R., Mullen, R.L., Yin, Y., Kahn, H., Stemmer, S. and Heuer, A.H., *Adv. Appl. Mech.*, 1997, **12**, 915-22.
23. Bravman, J.C. and Sinclair, R., *J. Electron. Micr. Tech.*, 1984, **1**, 53.
24. Ashurst, W.R., Yau, C., Carraro, C., Maboudian, R. and Dugger, M.T., *JMEMS*, 2001, **10**, 41-49.
25. Van Arsdell, W., Ph.D., Massachusetts Institute of Technology, 1997.
26. Muhlstein, C.L., Howe, R.T. and Ritchie, R.O., *Mech. Mater.*, 2001, in review.

27. Sharpe, W.N., Jr., Yuan, B. and Edwards, R.L., in *Proceedings of 1997 International Mechanical Engineering Congress and Exposition*, eds. J.C. Suhling, K.M. Liechti, and S. Liu, ASME, New York, NY, 1997, pp. 113-16.
28. Mikkelsen, J.C., in *Oxygen, Carbon, Hydrogen and Nitrogen in Crystalline Silicon*, eds. J.C. Mikkelsen, S.J. Pearton, J.W. Corbett, and S.J. Pennycook, MRS, Pittsburgh, PA, 1986, pp. 3-5.
29. Hirsch, P.B., Howie, A., Nicholson, R., Pashley, D.W. and Whelan, M.J., *Electron Microscopy of Thin Crystals*, 2nd ed., R.E. Krieger Pub. Co., Malabar, Fl, 1977.
30. Taft, E.A., *J. Electrochem. Soc.*, 1988, **135**, 1022-23.
31. Lukes, F., *Surf. Sci.*, 1972, **30**, 91-100.
32. Raider, S.I., Flitsch, R. and Palmer, M.J., *J. Electrochem. Soc.*, 1975, **122**, 413-18.
33. Lu, Z.H., Sacher, E. and Yelon, A., *Phil. Mag. B*, 1988, **58**, 385-88.
34. Fargeix, A. and Ghibaudo, G., *J. Appl. Phys.*, 1983, **54**, 7153-58.
35. Fargeix, A., Ghibaudo, G. and Kamarinos, G., *J. Appl. Phys.*, 1983, **54**, 2878-80.
36. Fargeix, A. and Ghibaudo, G., *J. Phys. D.*, 1984, **17**, 2331-36.
37. Fargeix, A. and Ghibaudo, G., *J. Appl. Phys.*, 1984, **56**, 589-91.
38. Kao, D., McVittie, J.P., Nix, W.D. and Saraswat, K.C., *IEEE Trans. Elect. Dev.*, 1987, **ED-34**, 1008-17.
39. Kao, D.B., McVittie, J.P., Nix, W.D. and Saraswat, K.C., *IEEE Trans. Elect. Dev.*, 1988, **ED-35**, 25-37.
40. Paul, W. and Warschauer, D.M., *Solids Under Pressure*, , McGraw-Hill, New York, NY, 1963.
41. Dill, S.J., Bennison, S.J. and Dauskardt, R.H., *J. Am. Ceram. Soc.*, 1997, **80**, 773-76.
42. ASTM, *E 647 Standard Test Method for Measurement of Fatigue Crack Growth Rates*, , Annual Book of ASTM Standards, ASTM, West Conshohocken, PA, 2001, vol. 03.01.
43. Hutchinson, J.W. and Suo, Z., *Adv. Appl. Mech.*, 1992, **29**, 63-163.
44. Lathabai, S., Yiu-Wing, M. and Lawn, B.R., *J. Am. Ceram. Soc.*, 1989, **72**, 1760-63.
45. Wiederhorn, S.M., in *Advances in Fracture Research*, eds. S.R. Valluri, D.M.R. Taplin, R. Ramo Rao, J.F. Knott, and R. Dubey, Pergamon Press, New York, NY, 1984, p. 613.

46. Dauskardt, R.H., *Acta Metal. Mater.*, 1993, **41**, 2765-81.
47. Lathabai, S., Rödel, J. and Lawn, B.R., *J. Am. Ceram. Soc.*, 1991, **74**, 1340-48.
48. Gilbert, C.J., Cao, J.J., MoberlyChan, W.J., DeJonghe, L.C. and Ritchie, R.O., *Acta Mater.*, 1996, **44**, 3199-14.
49. Asoo, B., McNaney, J.M., Mitamura, Y. and Ritchie, R.O., *J. Biomed. Mater. Res.*, 2000, 488-91.
50. Chen, C.P. and Leipold, M.H., *Amer. Cer. Soc. Bull.*, 1980, **59**, 469-72.
51. Lawn, B.R., Hockey, B.J. and Wiederhorn, S.M., *J. Mater. Sci.*, 1980, **15**, 12.
52. Chiao, Y.H. and Clarke, D.R., *Acta Metal.*, 1989, **37**, 203-19.
53. Ashurst, W.R., Yau, C., Carraro, C., Howe, R.T. and Maboudian, R., in *Hilton Head Solid-State Sensor and Actuator Workshop*, Transducers Res. Found, Hilton Head, SC, 2000, pp. 320-23.

FIGURES

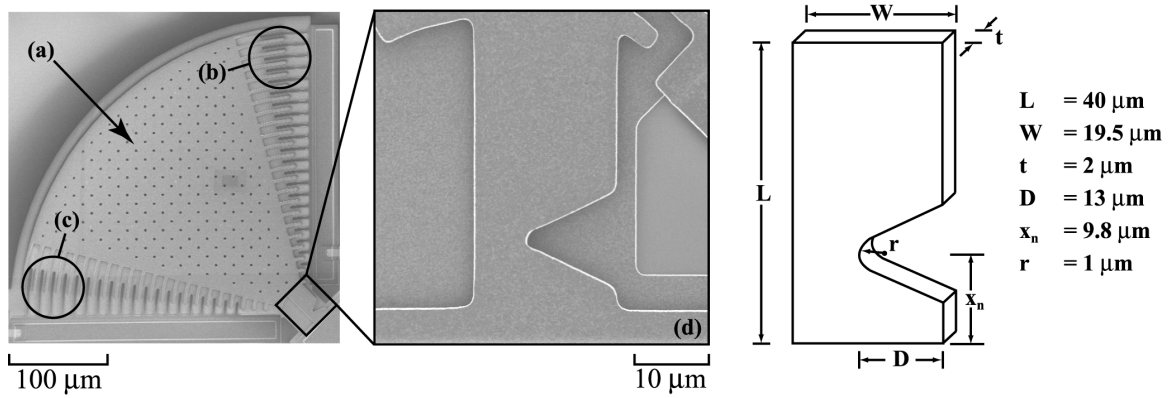


Fig. 1. Scanning electron micrograph of the fatigue life characterization structure and notched cantilever beam specimen used in this investigation. The (a) mass, (b) comb drive actuator, (c) capacitive displacement sensor, and (d) notched cantilever beam specimen are shown. The nominal dimensions of the specimen are as indicated in the schematic.

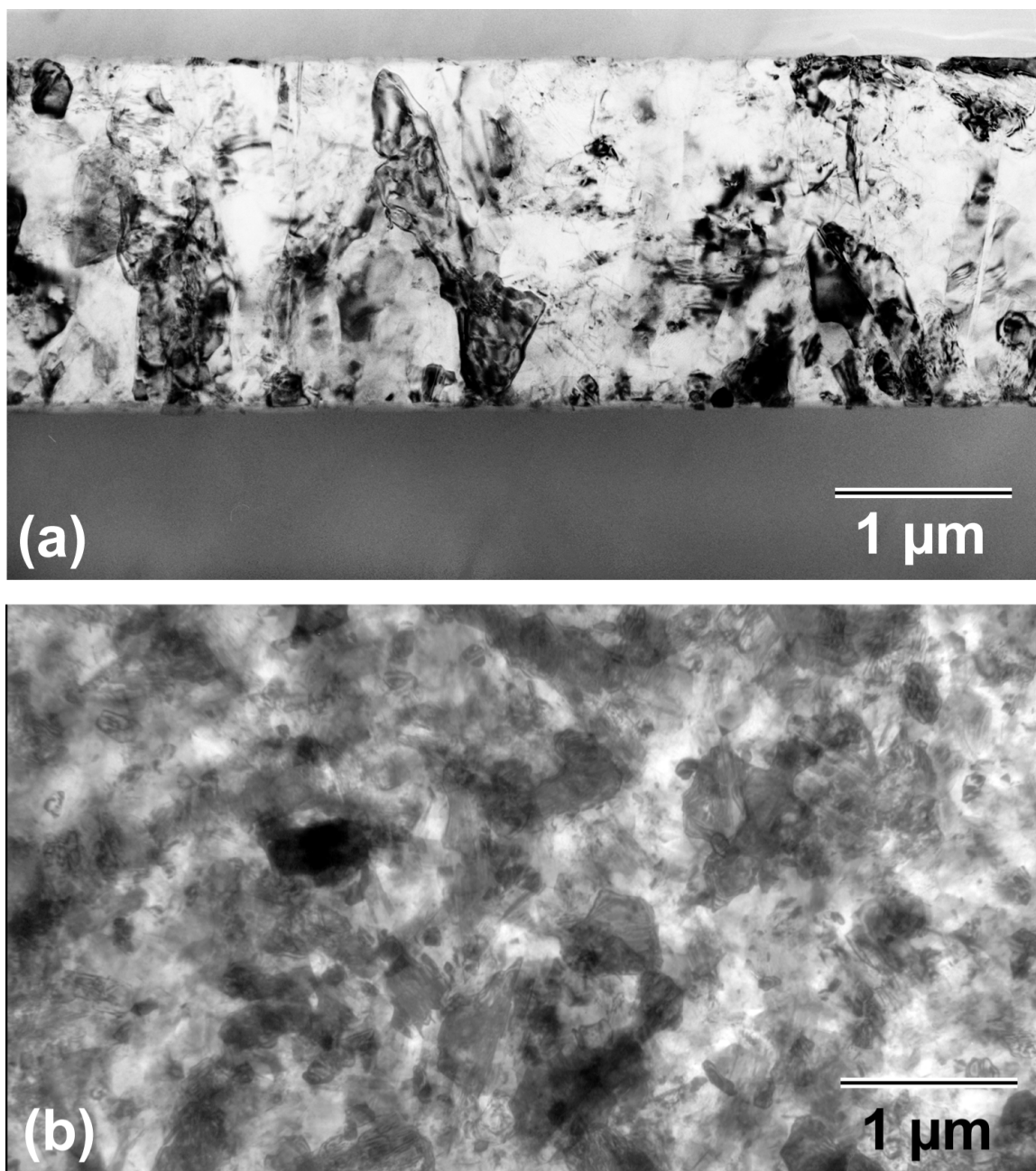


Fig. 2. Microstructure of the polycrystalline silicon structural film. (a) A typical cross sectional TEM image of the through-thickness microstructure and (b) plan view, full-thickness, HVTEM (1 MeV) image of the microstructure are shown.

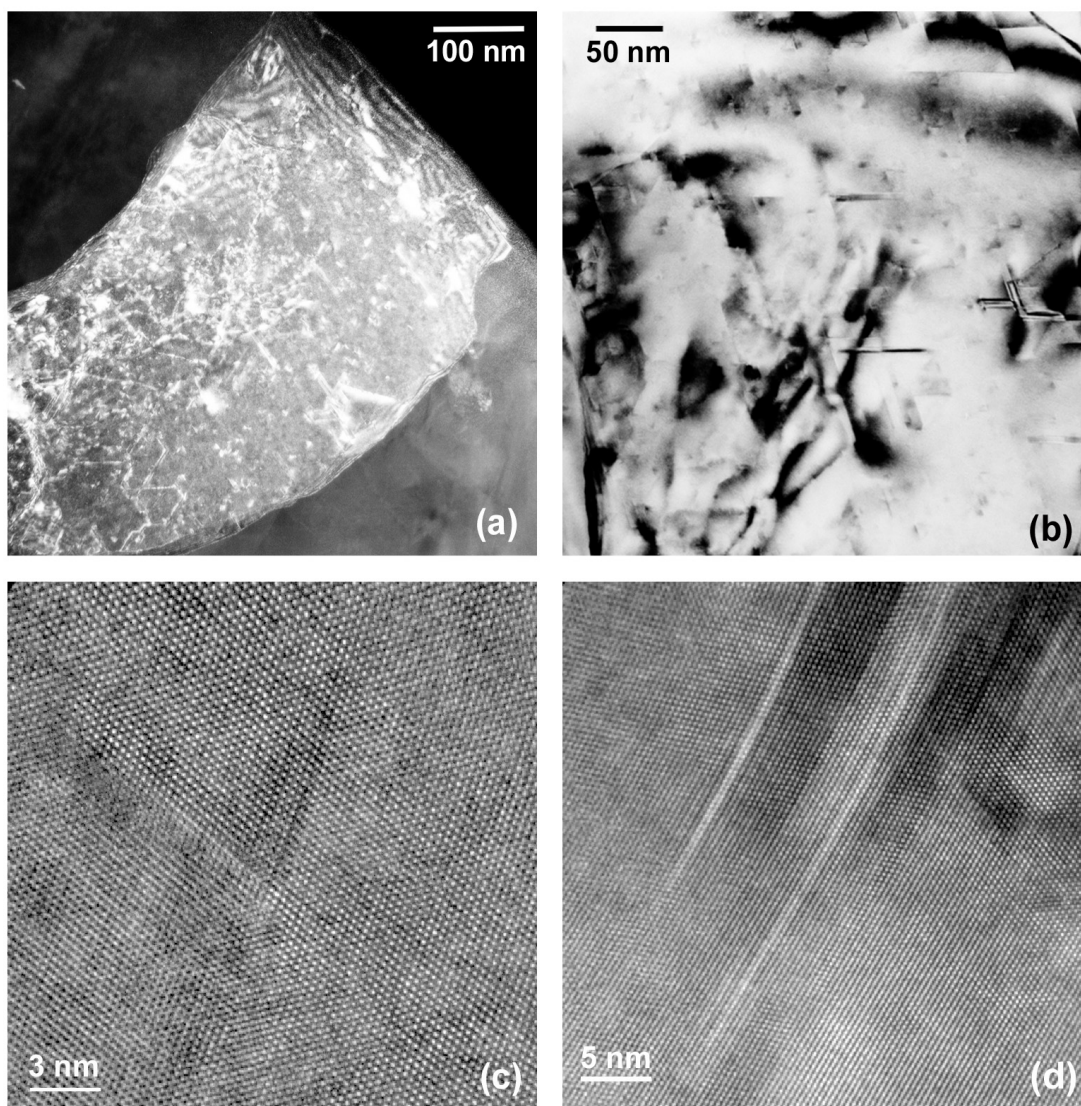


Fig. 3. TEM images of defect types, showing: (a) a representative polycrystalline silicon grain shown in weak beam dark field, (b) 220 bright field image of the interior of the grain to highlight microtwins, stacking faults, and Lomer-Cottrell dislocation locks, (c) high resolution image of a Lomer-Cottrell lock, and (d) high resolution image of microtwins.

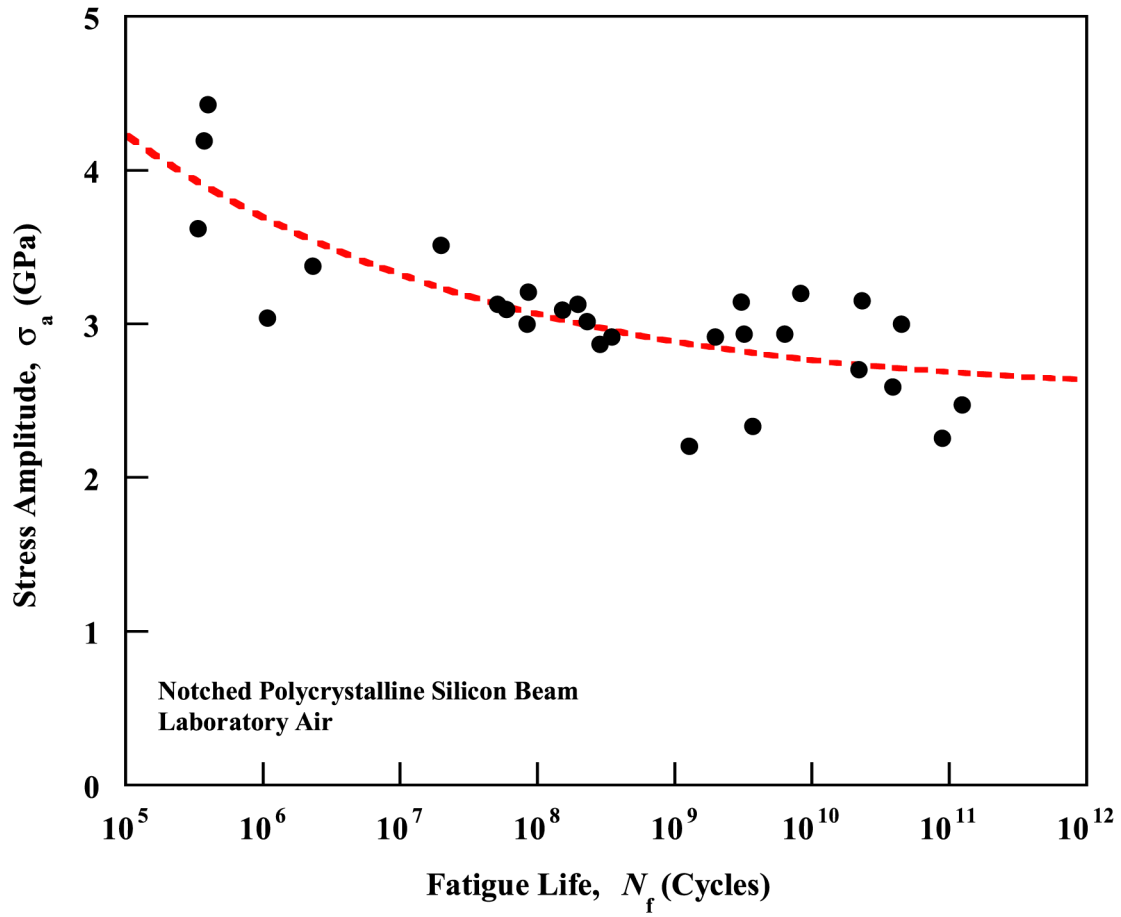


Fig. 4. Typical stress-life (S/N) fatigue behavior of the 2 μm-thick, polycrystalline silicon at 40 kHz in moist room air under fully reversed, tension-compression loading [4, 6].

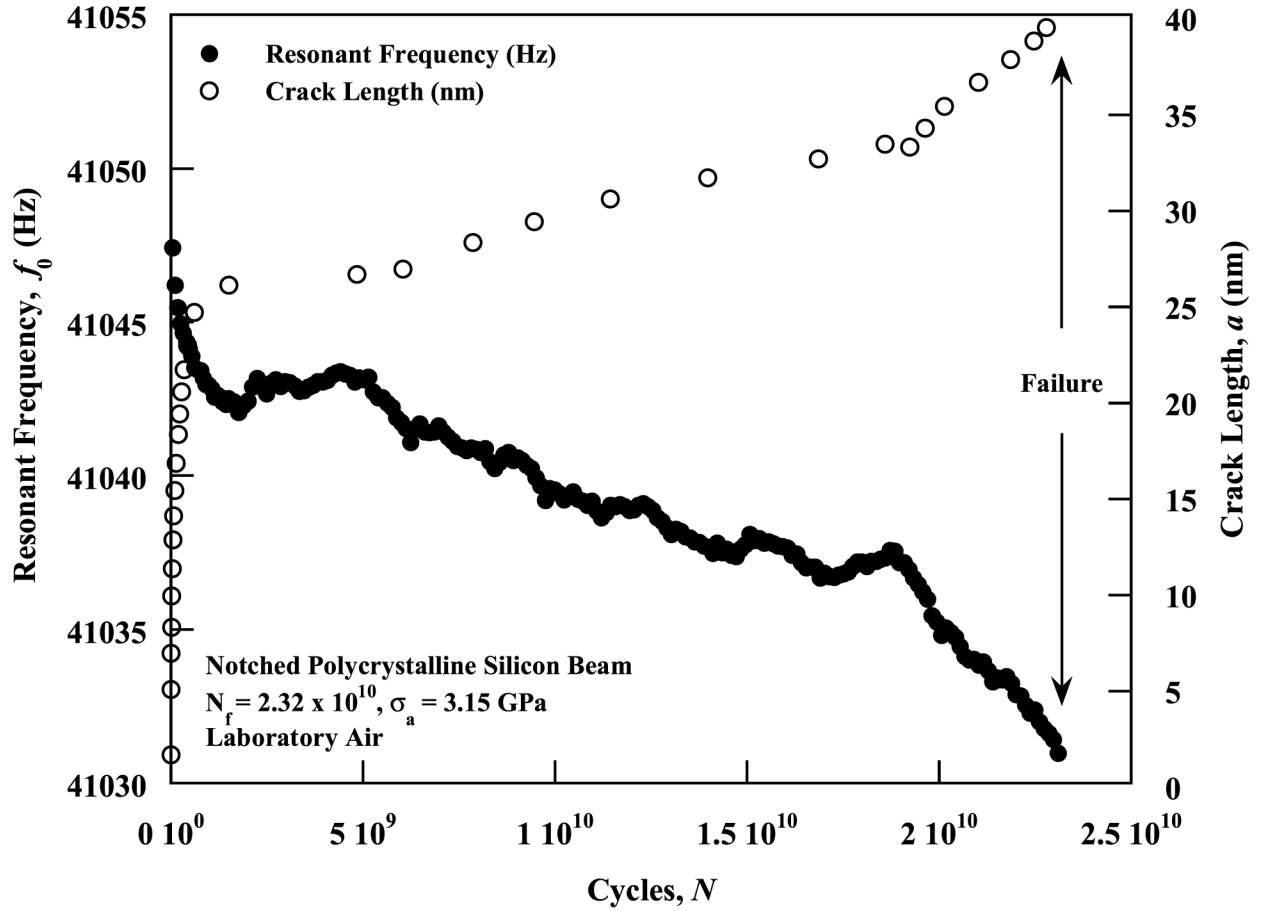


Fig. 5. Damage accumulation in polycrystalline silicon, shown by experimentally measured decrease in resonant frequency, f_{crack} , with time during the fatigue test ($N_f = 2.23 \times 10^{10}$ cycles at $\sigma_a = 3.15$ GPa, and the corresponding computed increase in crack length a).

Fig. 6. Fractography of failures in polysilicon films, showing (a) SEM and (b) HVTEM image of the crack trajectory out of the notch (in an unthinned specimen). (c) SEM images of the transgranular cleavage fracture surfaces of a long-life fatigue test ($N_f = 3.8 \times 10^{10}$ cycles at $\sigma_a = 2.59$ GPa). Horizontal arrow in (a) indicates the direction of crack propagation. Note the fine, needle-like features and debris on the fracture surface in (c).

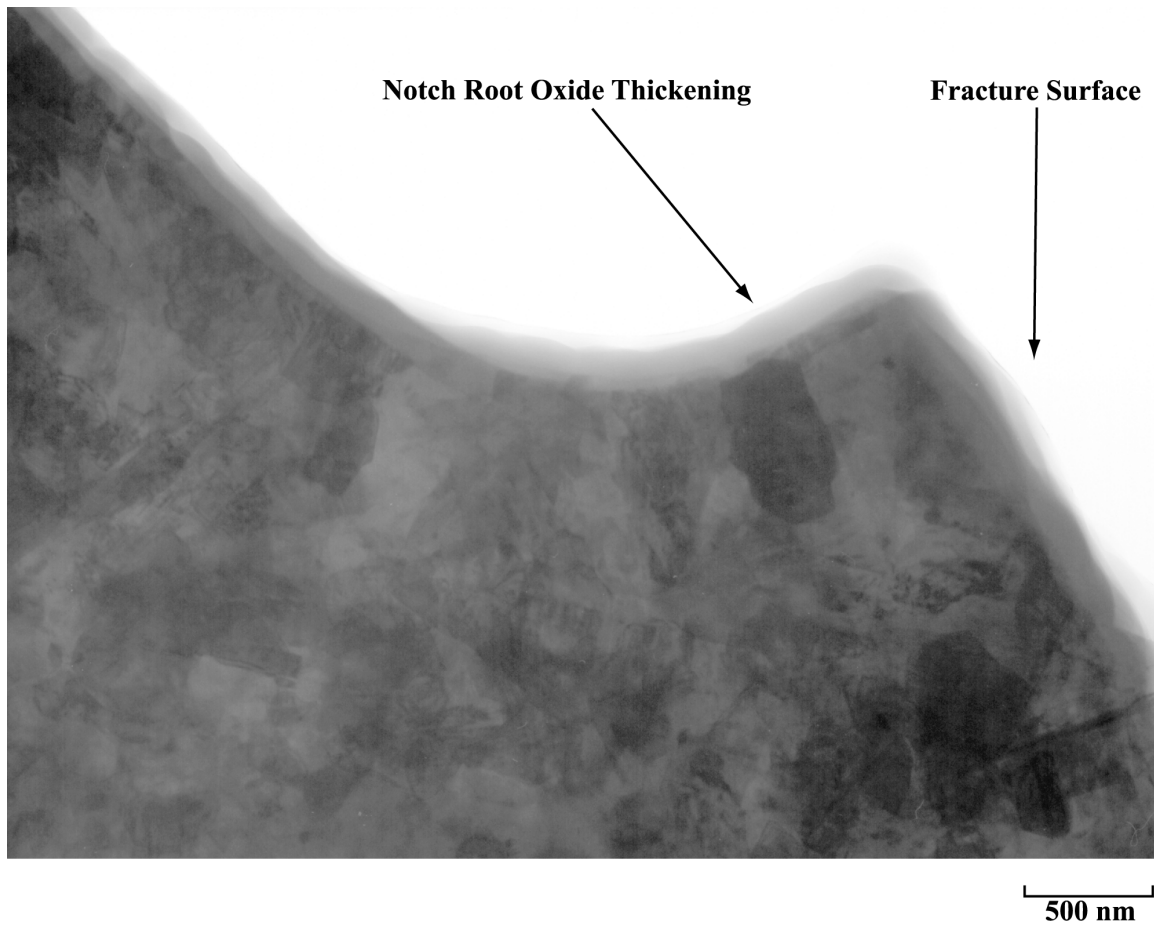


Fig. 7. HVTEM image of the notch region in an unthinned polysilicon test sample, showing enhanced oxidation at the notch root after cycling for 3.56×10^9 at $\sigma_a = 2.26$ GPa.

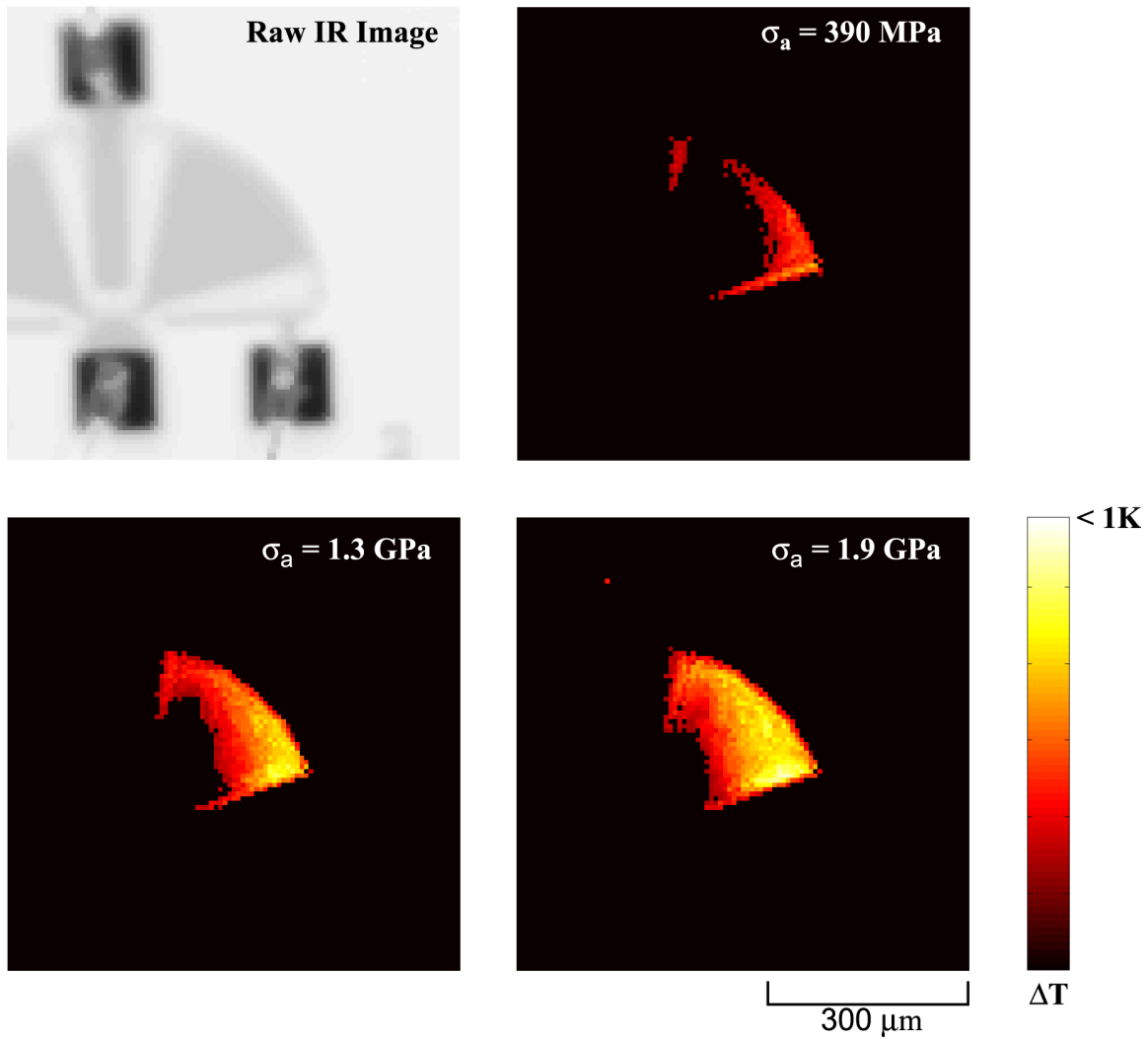


Fig. 8. High resolution (20 mK) infrared (IR) images of the fatigue characterization structure at rest and at increasing stress amplitude at 40 kHz. Maximum temperature variations were less than 1K above ambient and were not measurable in the notched cantilever beam specimen.

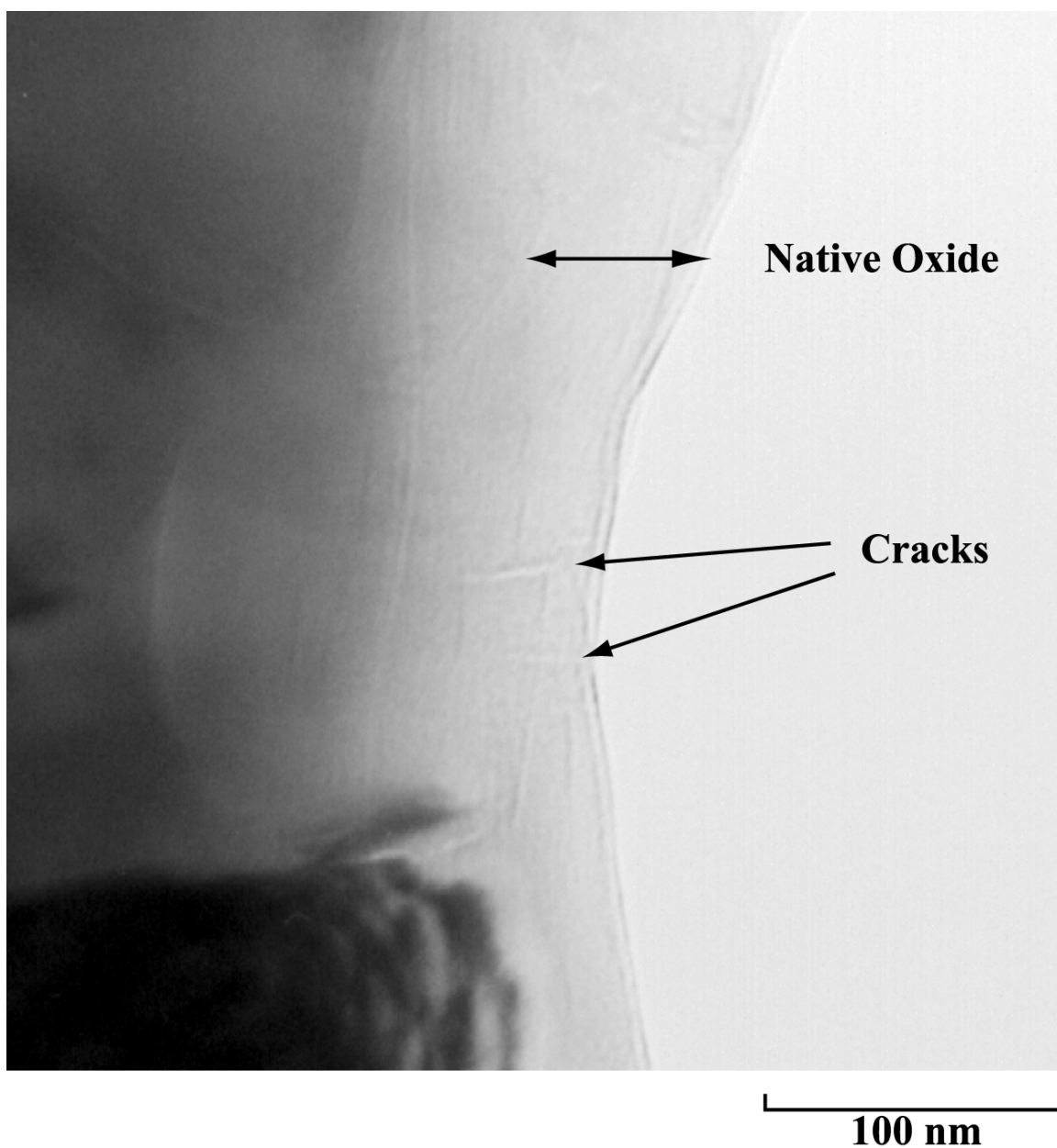


Fig. 9. HVTEM image showing stable cracks, ~ 50 nm in length, in the native oxide formed during cyclic loading of a notched, polycrystalline silicon beam. Testing of this sample was interrupted after $N = 3.56 \times 10^9$ cycles at a stress amplitude $\sigma_a = 2.51$ GPa. Image was intentionally defocused to facilitate the observation of the cracks.

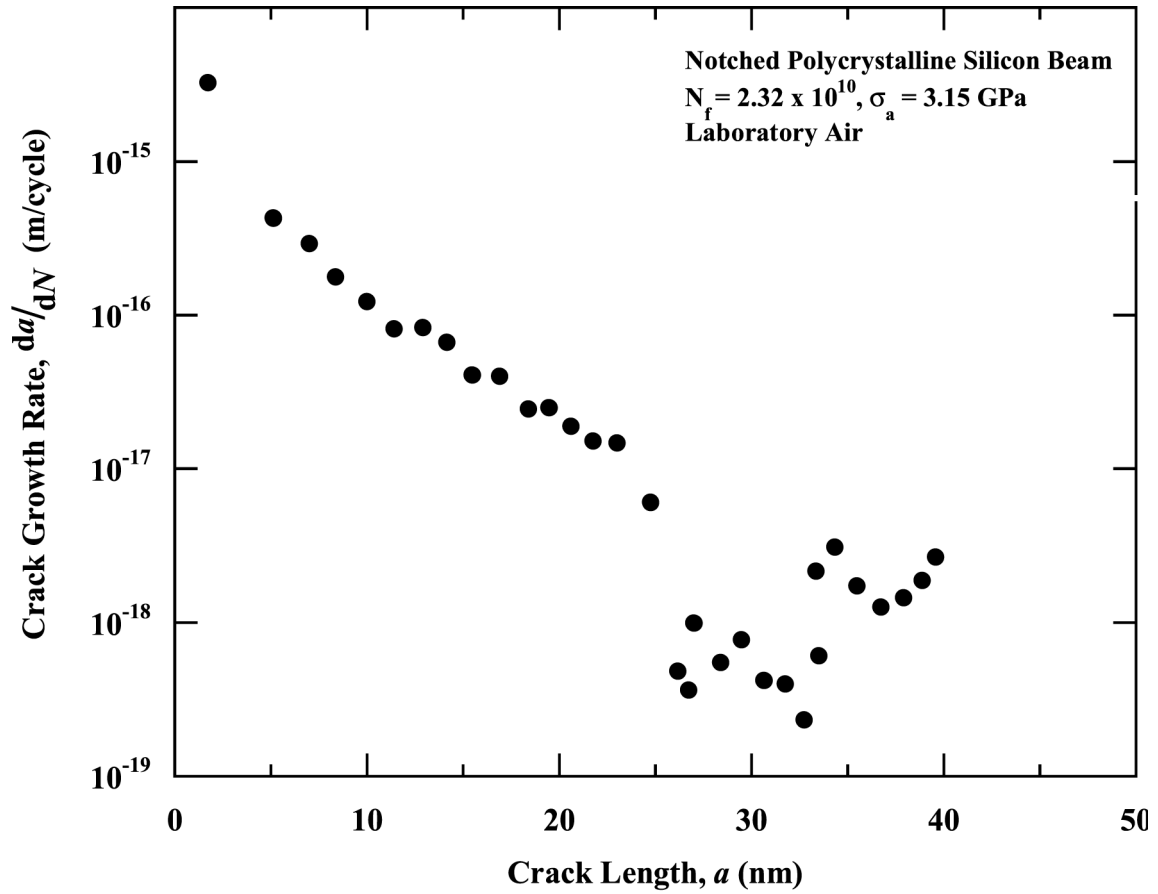


Fig. 10. Computed fatigue-crack growth rates, da/dN , as a function of the crack length, a , during a fatigue test of a polycrystalline silicon thin film ($N_f = 2.3 \times 10^{10}$ cycles at $\sigma_a = 3.15$ GPa). Growth rates were determined from the change in specimen compliance monitored throughout the test. Note that the entire fatigue process of crack initiation and growth until the onset of catastrophic failure occurs for crack sizes below ~ 50 nm, i.e., within the native oxide layer.

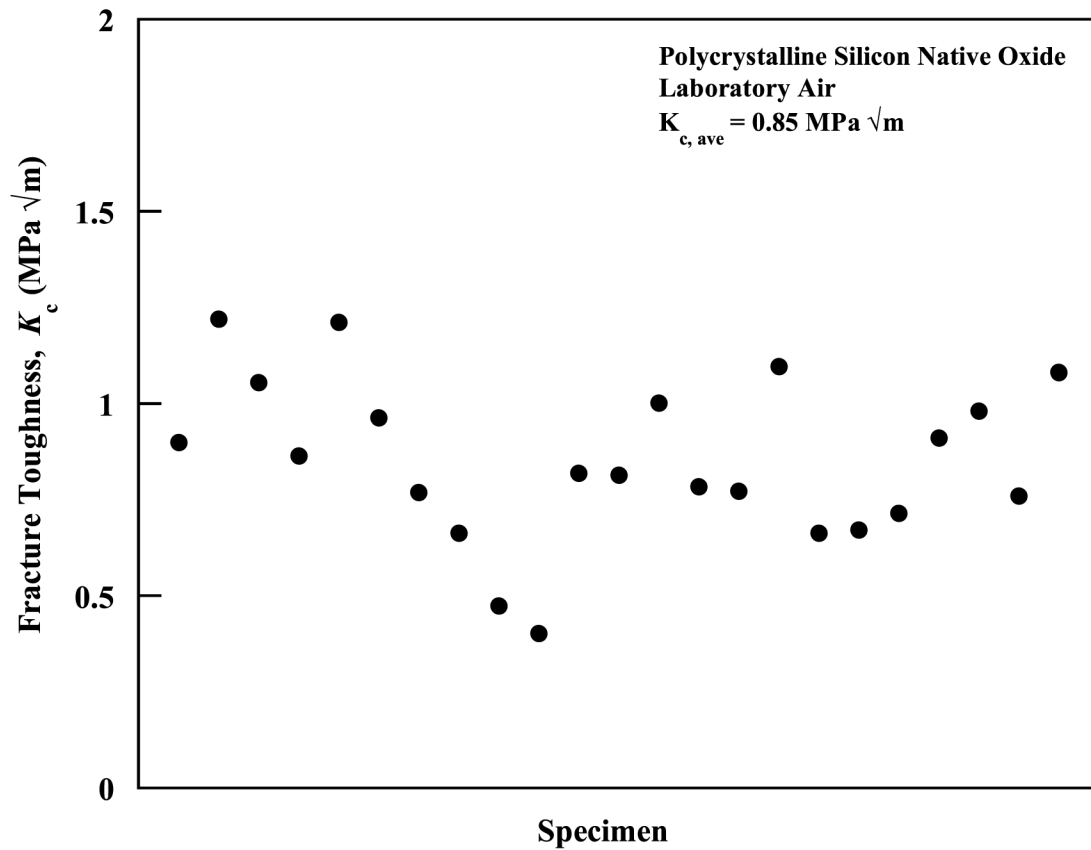


Fig. 11. Computed fracture toughness, K_c , values determined from the estimated crack length immediately prior to failure, i.e., the critical crack size, a_c , for the given applied stress amplitude. The average fracture toughness of $0.85 \text{ MPa} \sqrt{\text{m}}$ is consistent with failure within the native oxide on polycrystalline silicon at room temperature.

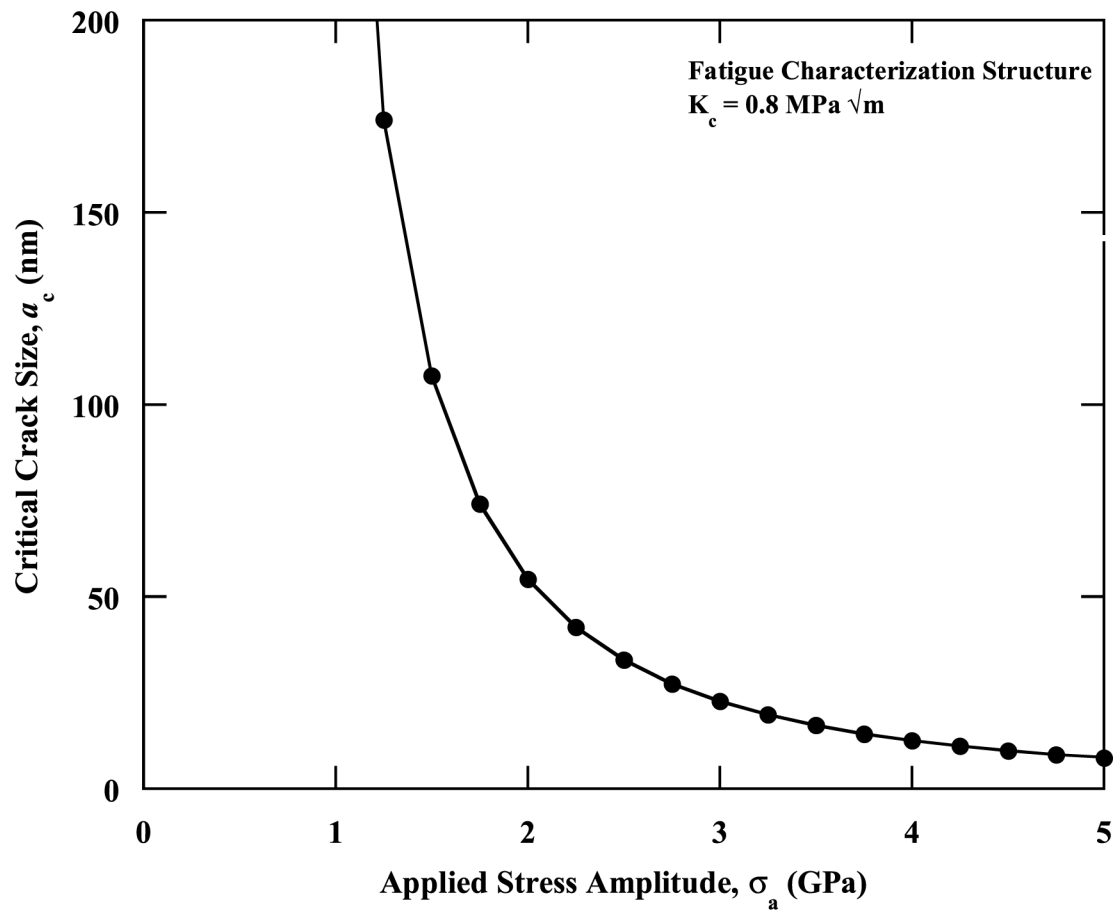


Fig. 12. Computed estimates of the critical crack size, a_c , as a function of the applied stress amplitude, σ_a , in the polycrystalline silicon fatigue characterization structure. Critical crack sizes for the stress amplitudes used in the present tests ($\sigma_a \sim 2$ to 4 GPa) are less than ~ 50 nm, indicating that the onset of final failure of the structure occurs at crack sizes within the native oxide reaction layer.

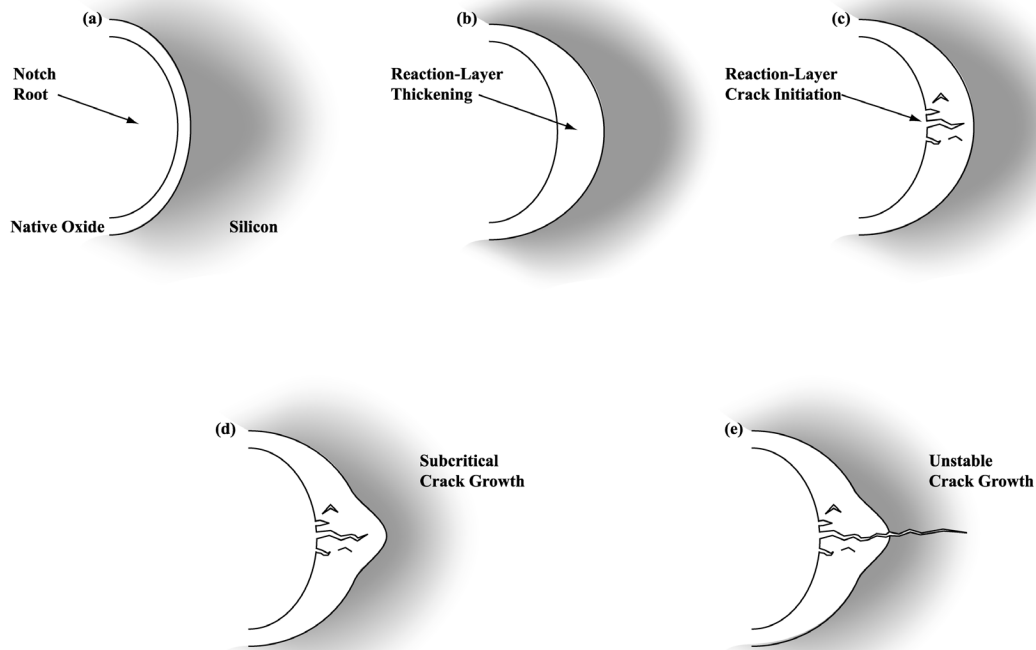


Fig. 13. Schematic illustrations of the reaction-layer fatigue mechanism at the notch of the polycrystalline silicon cantilever beam. (a) Reaction layer (native oxide) on surface of the silicon. (b) Localized oxide thickening at the notch root. (c) environmentally-assisted crack initiation in the native oxide at the notch root. (d) Additional thickening and cracking of reaction layer. (e) Unstable crack growth in the silicon film.

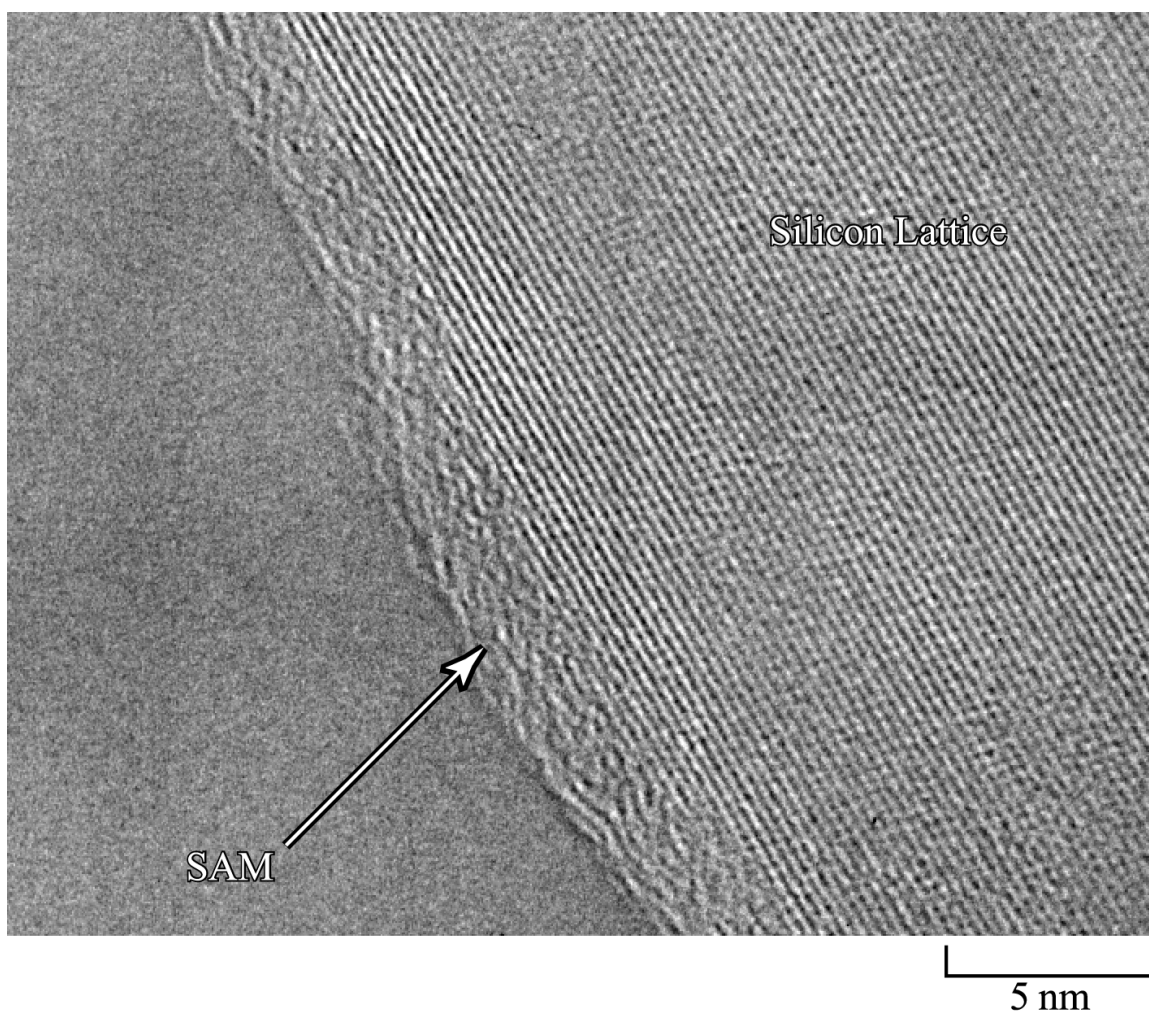


Fig. 14. HVTEM image showing a 1-octadecene self-assembled monolayer coating the root of the polysilicon notch. The lattice fringes of the silicon are clearly visible under the ~ 3 nm layer that has suppressed the formation of the native oxide layer on the silicon surface.

Fig. 15. Comparison of the fatigue behavior of uncoated and SAM-coated polycrystalline silicon thin films, showing (a) the respective S/N curves and (b) accumulated fatigue damage in terms of the change in natural frequency of the sample, f_{crack} , normalized by the natural frequency at the start of the test, f_0 . Note the reduced susceptibility of the coated polysilicon films to fatigue failure in (a), and the significantly enhanced life (by two orders of magnitude) compared to uncoated polysilicon at compared applied stress amplitudes in (b).

